Analytica Chimica Acta 1025 (2018) 99–107

Contents lists available at ScienceDirect

Analytica Chimica Acta

journal homepage: www.elsevier.com/locate/aca

A label-free photoelectrochemical biosensor for urokinase-type plasminogen activator detection based on a g-C_3N_4/CdS nanocomposite

Xing-Pei Liu, Jing-Shuai Chen, Chang-jie Mao*, He-Lin Niu, Ji-Ming Song, Bao-Kang Jin

Anhui Province Key Laboratory of Chemistry for Inorganic/Organic Hybrid Functionalized Materials, School of Chemistry & Chemical Engineering, Anhui University, Hefei, 230601, China

HIGHLIGHTS

- A novel, lable-free photoelectrochemical biosensor was constructed for urokinase-type plasminogen activator (u-PA) detection.
- Urokinase-type plasminogen activator (u-PA) was first time detected by photoelectrochemical technique.
- The proposed photoelectrochemical protocol presented ultrahigh sensitivity, reproducibility, specificity and stability.

GRAPHICAL ABSTRACT

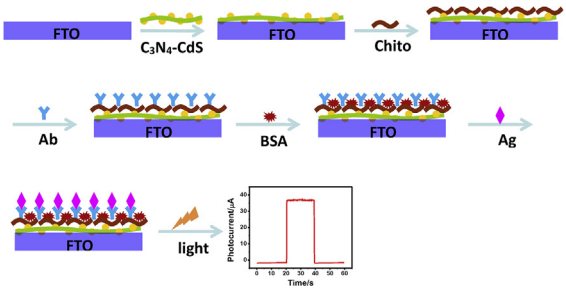

ARTICLE INFO

Article history:
Received 15 February 2018
Received in revised form
16 April 2018
Accepted 20 April 2018
Available online 23 April 2018

Keywords:
Urokinase-type plasminogen activator
Biosensor
Photoelectrochemistry
C_3N_4/CdS

ABSTRACT

Herein, we established a novel ultrasensitive photoelectrochemical biosensor for detecting urokinase-type plasminogen activator (u-PA), based on a g-C_3N_4/CdS nanocomposite. The prepared nanocomposite was characterized by transmission electron microscopy, X-ray photoelectron spectroscopy, ultraviolet–visible absorption spectroscopy, and Fourier transform infrared spectroscopy, thus indicating that the nanocomposite was prepared successfully. In the typical process, the prepared nanocomposite was deposited on the surface of a bare FTO electrode. After being air-dried, the g-C_3N_4/CdS nanocomposite modified electrode was successively incubated with antibody against urokinase-type plasminogen activator and the blocking agent BSA to produce a photoelectrochemical biosensor for u-PA. In the presence of target u-PA antigen, the photocurrent response of the prepared biosensor electrode decreased significantly. The proposed novel photoelectrochemical biosensor exhibited good sensitivity, specificity, and reproducibility for u-PA detection, and a low detection limit of 33 fg mL^{-1}, ranging from 1 μg mL^{-1}–0.1 pg mL^{-1}. The proposed strategy should provide a promising method for detection of other biomarkers.

1. Introduction

Urokinase-type plasminogen activator (u-PA), a member of the serine protease family, functions in the human plasminogen activation system and is critical for tissue degradation and remodeling, cell migration, extravascular fibrinolysis, and cancer invasion and

* Corresponding author.
E-mail address: maochangjie@sina.com (C.-j. Mao).

https://doi.org/10.1016/j.aca.2018.04.051
0003-2670/

metastasis [1–3]. The u-PA is associated with many diseases including spontaneous intracerebral hemorrhage, tuberous sclerosis complex 2, pancreatic ductal adenocarcinoma, male infertility, lymphangioleiomyomatosis, small-cell lung carcinoma, gastroesophageal cancer, gastric cancer, and heart, kidney, and liver diseases [1–8]. As a clinical diagnostic biomarker, u-PA is overexpressed in many physiological and pathological processes, and it catalyzes the conversion of plasminogen to plasmin [9]. The u-PA binds its receptor on the cell surface and promotes the invasion and metastasis of tumor cells [10,11]. Because higher expression of u-PA is seen on tumor cells, the monitoring of u-PA is important for tumor screening. To date, many efforts have been made towards detecting u-PA [12]. For example, Luan et al. proposed a fluorescent nanoprobe for detecting u-PA [13]. Sinharay et al. detected u-PA with a catalyCEST MRI contrast agent [9]. Čejková et al. also detected activity of u-PA with the use of AFC substrates [14]. Despite these efforts, there are still some restrictions, such as complex operation and limited sensitivity. Therefore, it is necessary to develop a simple and sensitive method for detection of u-PA. As far as we know, few studies have focused on the detection of u-PA through a photoelectrochemical biosensor.

Photoelectrochemical biosensors are a rapidly developing analytical technique for biomarker detection. They provide the advantages of both photochemistry and electrochemistry, such as high sensitivity, low cost, low background response, use of simple equipment, and easy operation [15–22]. The basic photoelectrochemical process refers to photon-electricity conversion, in which photoactive materials are excited by a light source, thus resulting in charge separation and transfer, oxidation-reduction reactions, and generation of a photocurrent signal [23–27]. In the conventional photoelectrochemical process, the photoactive materials are of great importance. The non-metal semiconductor photoactive material, graphite-like carton nitride (g-C_3N_4), has attracted a great deal of attention because of its excellent photoactivity, relatively low band-gap (~2.69 eV) [28,29], high chemical and thermal stability [18], good biocompatibility [17], environmental friendliness, and raw material availability. Despite these advantages, the application of g-C_3N_4 in photoelectrochemistry has been hindered by the high recombination rate of photo-generated electron-hole pairs [18,28]. To overcome this drawback and extend the potential applications, some modifications for g-C_3N_4 are necessary. CdS quantum dots (QDs), a commonly used semiconductor nanomaterial, have been extensively applied in photoelectrochemical sensors. Despite a narrow band gap (~2.4 eV), CdS QDs still have many disadvantages. However, the direct band gap of g-C_3N_4 can match the energy levels of CdS QDs, thus effectively suppressing the recombination of photo-generated electron-hole pairs and extending their light-capturing ability [17,18]. Therefore, in this work, g-C_3N_4 was combined with CdS to form a nanocomposite, which in turn was used to construct a photoelectrochemical biosensor.

We developed an ultrasensitive photoelectrochemical biosensor for detecting urokinase-type plasminogen activator (u-PA), based on g-C_3N_4/CdS nanocomposites. As shown in Scheme 1, the prepared g-C_3N_4/CdS nanocomposites were deposited on a bare fluorine-doped tin oxide (FTO) electrode pretreated with PDDA, and a uniform nano-film was formed after air-drying. Then the g-C_3N_4/CdS nanocomposite-modified electrode was used as the matrix of the biosensor. Next, chitosan was deposited on the surface of the g-C_3N_4/CdS nanocomposites. Subsequently, glutaraldehyde was coated on the modified electrode to connect the chitosan and anti-u-PA antibody. Finally, BSA was used as blocking agent to block unbound sites. Then the prepared biosensor electrode was used for u-PA detection. The proposed photoelectrochemical biosensor was found to provide a sensitive, specific, reproducible and stable strategy for detection of other biomarkers.

2. Experiment

2.1. Materials and reagents

Melamine, cadmium chloride ($CdCl_2$) and 3-mercaptopropionic acid (MPA) were purchased from Aladdin Reagent Co. Ltd (Shanghai, China). Thioacetamide (TAA) were obtained from Macklin Biochemical Co. Ltd (Shanghai, China). Poly (diallyldimethylammonium chloride) (PDDA, Mw = 200000–350000, 20 wt% in H_2O), bovine serum albumin (BSA) were obtained from Sigma-Aldrich Co. Ltd (Shanghai, China). Glutaraldehyde (GLD, 50% aqueous solution) and ascorbic acid (AA) were acquired from Shanghai Sangon Biological Engineering Technology Co. Ltd (Shanghai, China). MUC1 was synthesized by Shanghai Apeptide Co., Ltd. (Shanghai, China). Urokinase-type plasminogen activator (u-PA), interleukin-6 (IL-6), carcinoembryonic (CEA) and cytochrome C (Cyt C) were provided by Beijing Biosynthesis

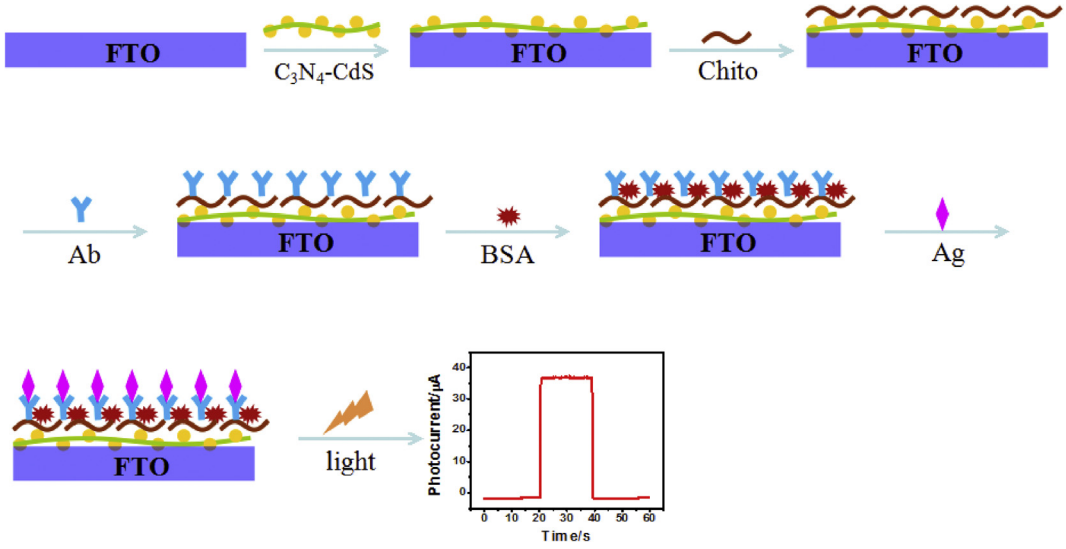

Scheme. 1. Schematic diagram of the entire fabrication process for the photoelectrochemical sensor.

Biotechnology Co. Ltd (Beijing, China). All reagents were analytical pure and without purification before used. Ultrapure water (18 MΩ/cm) which employed in the whole work was obtained from an AK Exceed-E-V lab pure water system (Chengdu, China). 0.1 M phosphate buffered saline (PBS, pH 7.4, 0.1 M AA was included) was made by NaH_2PO_4, Na_2HPO_4, NaCl and AA served as the electrolyte in the photoelectrochemical test. 10 mM of phosphate buffered saline (pH 7.4; 136.89 mM of NaCl, 2.67 mM of KCl, 8.24 mM of Na_2HPO_4, 1.76 mM of KH_2PO_4) was applied to prepare u-PA and washing buffer, and the blocking agent was 10 mM of PBS (pH 7.4) including 1% BSA.

2.2. Instrumentations

Transmission electron microscopy (TEM) images were carried out with a JEM-2100 transmission electron microcopy (JEOL Ltd., Japan). X-ray photoelectron spectroscopy (XPS) was performed with an ES-CALAB 250 X-ray photoelectron spectroscopy (Thermo Ltd, USA). Ultraviolet–visible (UV–vis) absorption spectra were recorded on a UV-3600 UV spectroscopy (Shimadzu Ltd, Japan). Infrared spectroscopy was recorded on a Fourier transform infrared spectrometer (FTIR, NEXUS-870, Nicolet Instrument Co., USA). The photoelectrochemical measurements were performed on a CHI 660D electrochemical workstation (CH Instruments, China) with a traditional three electrode system: a modified FTO as working electrode, a Pt electrode as counter electrode, Ag/AgCl (saturated KCl) as reference electrode. The light source was xenon lamp (Nanjing Yanan Special Lighting Factory, China). EIS performed on a Thales electrochemical workstation (Zahner-elektrik GmbH & Co., Germany) with the three electrode system consisted of a platinum electrode, calomel electrode, and the modified FTO. The electrolyte was 0.01 M of PBS (pH 7.4) including 0.1 M of KCl and 2 mM of $K_3[Fe(CN)_6]/K_4[Fe(CN)_6]$ (1:1), the frequency was ranged from 10 mHz to 100 KHz, and the amplitude was 5 mV.

2.3. Synthesis of g-C_3N_4 and g-C_3N_4/CdS nanocomposite

The synthetic procedures of g-C_3N_4 was based on the previous report with some modifications [30,31]. 10 g of melamine was calcined at 550 °C for 4 h in air atmosphere. After cooling to room temperature, the yellow bulk-C_3N_4 was grinded into powder. Then the prepared powder was heated at 500 °C for another 2 h. The obtained powder was dispersed in uptrapure water with a concentration of 2.5 mg mL^{-1} and ultrasonicated for 12 h. Then the prepared suspension was centrifuged at 6000 rpm for 10 min and removed the residual bulk g-C_3N_4. The obtained milky suspension was stored in a refrigerator at 4 °C before use.

The g-C_3N_4/CdS nanocomposite was synthesized according to the literature method [32]. Firstly, 172 μL of MPA and 0.1467 g of $CdCl_2$ were added to 40 mL of prepared g-C_3N_4 suspension and stirred under N_2 atmosphere for 30 min to remove O_2. Next, 1.0 M NaOH was added to adjust the pH of the solution to 11.0. Then 40 mL 20 mM of TAA solution was injected into above mixture solution to obtain a precursor solution, and the reaction mixture was refluxed under highly pure N_2 protection for 2 h at 80 °C. After cooling, 1 mL of the resulting g-C_3N_4/CdS nanocomposite solution was washed with absolute ethanol and centrifuged at 8000 rpm for 10 min, and the final fixed volume was 4 mL. The prepared nanocomposite was stored in a refrigerator at 4 °C before use.

2.4. Preparation of the FTO/g-C_3N_4/CdS electrode

In preparation, FTO glasses (Shenzhen Huananxiangcheng Technology Co. Ltd, China, sheet resistance ≤15 Ω $square^{-1}$) were cleaned by ultrasonic treatment for 15 min with acetone, water and ethanol respectively, and dried at 60 °C in atmosphere overnight. Next, the bare FTO electrode was pretreated with 1% PDDA for 1 h, then rinsed with 10 mM PBS (pH = 7.4). After that, 30 μL of the prepared g-C_3N_4/CdS nanocomposite was droped on the surface of the bare FTO electrode. After drying in air, the modified electrode was rinsed with ultrapure water and dried with nitrogen, then the modified electrode was prepared successfully.

2.5. Fabrication of the biosensor and target u-PA analysis

10 μL chitosan solution (0.1 wt%, aqueous solution) was dropped onto FTO/g-C_3N_4/CdS electrode surface and dried in air. After rinsed with ultrapure water, 30 μL of 5% glutaraldehyde (GLD) solution was droped on the electrode surface at ambient temperature and kept for 0.5 h. Then the electrode was washed with ultrapure water several times. 30 μL of 0.01 mg mL^{-1} anti-u-PA antibody solutions were dropped onto the electrode and incubating at 4 °C overnight. After rinsed with PBS (10 mM, pH = 7.4), the electrode was blocked with 30 μL of 1% (w/v) BSA blocking agent at 37 °C for 1 h to cover nonspecified binding sites. At last, the resulting electrode was incubated with 30 μL of different concentrations of u-PA at 37 °C for 1 h and rinsed with PBS (10 mM, pH 7.4). The modified electrode was prepared for photoelectrochemical detection. Scheme 1 shows the whole fabricating steps of the photoelectrochemical biosensor.

2.6. Photoelectrochemical detection

The photoelectrochemical measurement was carried out in 0.1 M PBS (pH 7.4, 0.1 M AA was involved and acted as the sacrificial electron donor during the photocurrent measurement.) [33]. A 250 W Xe lamp served as the excitation light source, the light wavelength ranged from 280 to 1000 nm, and the light was switched on and off every 20 s. The impressed voltage was 0.0 V. Once the light irradiate on the photoelectrochemical electrodes, the photocurrent was recorded.

3. Results and discussion

3.1. Characterization of g-C_3N_4 and g-C_3N_4/CdS nanocomposites

The surface morphology of the g-C_3N_4 and g-C_3N_4/CdS nanocomposites was characterized by TEM. As shown in Fig. 1A, pure g-C_3N_4 exhibited an ultrathin lamellar nanosheet structure with a smooth surface. Fig. 1B shows that the CdS nanoparticles were homogeneously spread on the g-C_3N_4 nanosheet surface, and the g-C_3N_4/CdS nanocomposite surface was rough. The TEM results indicated that CdS nanoparticles were tightly coated on the surface of g-C_3N_4.

The optical properties of g-C_3N_4, CdS and g-C_3N_4/CdS nanocomposites were recorded by ultraviolet–visible absorption spectra (UV–vis) and infrared spectroscopy (IR). As shown in Fig. 1C, the characteristic absorption peak of pure g-C_3N_4 was approximately 322 nm, corresponding to previous reports (curve a) [34,35]. Pure CdS nanoparticles exhibited a broad absorption range below 500 nm and an evident absorption peak at 377 nm (curve b). The g-C_3N_4/CdS nanocomposite showed the characteristic absorption peaks of both g-C_3N_4 and CdS nanoparticles, thus indicating that CdS nanoparticles were coated on the surface of g-C_3N_4. Fig. 1D shows the FT-IR spectra of the above materials. The sharp absorption at 810 cm^{-1} resulted from the vibration of tri-*s*-triazine units. The broad absorption between 900 and 1800 cm^{-1} was ascribed to the stretching and rotation vibration of N (-C)$_3$ and C-NH-C. The peaks in the region of 3100–3400 cm^{-1} were attributed to N-H stretching vibration in primary and secondary amines (curve a) [36,37]. As shown in Fig. 1D, a characteristic peak at 634 cm^{-1} was

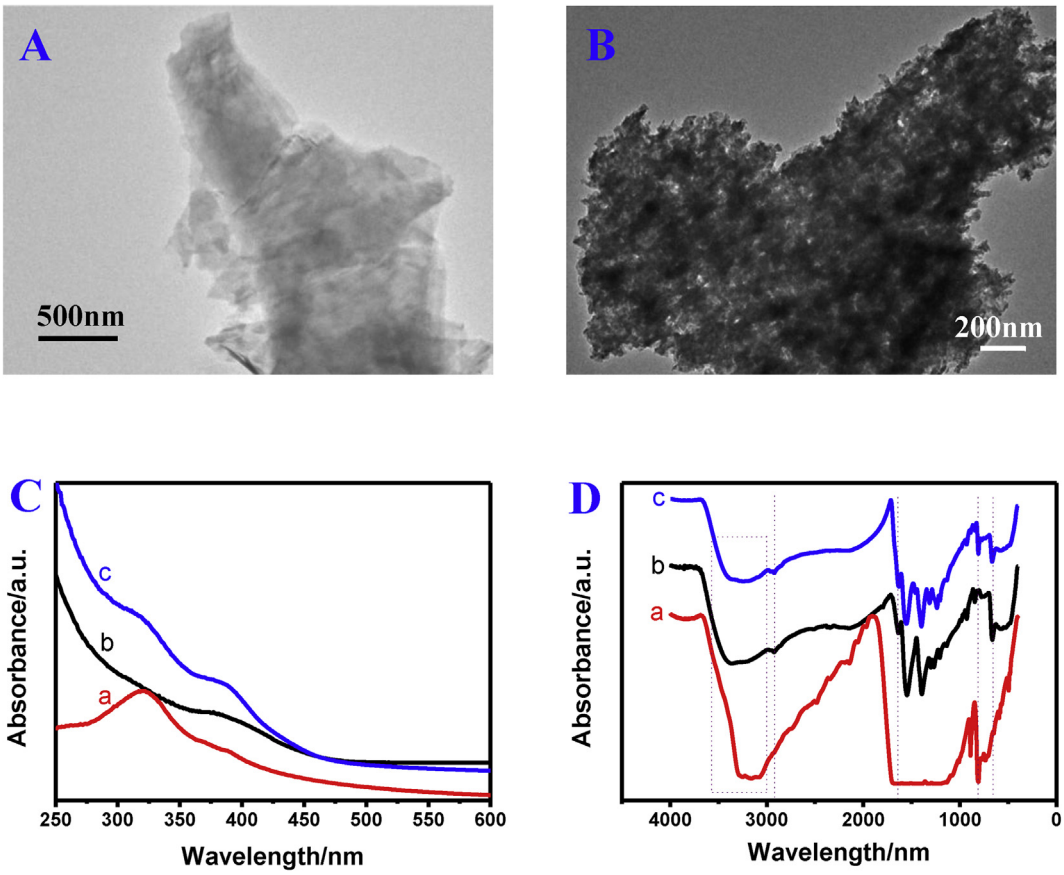

Fig. 1. (A) TEM image of g-C_3N_4, (B) TEM image of g-C_3N_4/CdS, (C) UV–vis and (D) FT-IR of (a) g-C_3N_4, (b) CdS, and (c) g-C_3N_4/CdS nanocomposites.

ascribed to the stretching vibration of Cd-S. A clear band at 1625 cm^{-1} was attributed to the bending vibration of O-H. The peak at 2925 cm^{-1} suggested the involvement of C-H and H-O groups in nanoparticles (curve b) [38–40]. The FT-IR spectrum confirmed that the g-C_3N_4/CdS nanocomposite was prepared successfully.

The surface composition and elemental analyses of the g-C_3N_4/CdS nanocomposite were performed using XPS. Fig. 2A shows the survey XPS spectrum analysis of the modified electrode, which indicated the C, N, Cd, and S elements in the prepared nanocomposite. Fig. 2B shows the high resolution spectrum of Cd 3d, in which the peaks located at 405 eV and 411.7 eV could be attributed to Cd 3d5/2 and Cd 3d3/2 respectively, thus confirming that Cd existed in a +2 oxidation state [41–43]. As shown in Fig. 2C, the binding energies of 161 eV, 162.2 eV and 161.9 eV in the high resolution XPS spectrum corresponded to the S 2p3/2 and S 2p1/2 peaks of S^{2-} in CdS nanoparticles, respectively. The binding energy of 163.15 eV was attributed to S-S [41,44]. Fig. 2D shows the high resolution spectrum of C 1s; the binding energy of 284.8 eV was ascribed to the C-C/C-H, and the binding energy of 288.15 was ascribed to the N-C=N of g-C_3N_4 [44]. As shown in Fig. 2E, the binding energies of 404.95 eV and 398.85 eV in the high resolution spectrum of N 1s were attributed to C-N-H and C-N=C [45].

3.2. Optimized conditions

To efficiently apply the proposed photoelectrochemical biosensor to target u-PA detection, several experimental parameters were optimized. Fig. 3 shows the optimized conditions for this experiment. As shown in Fig. 3A, the concentration of g-C_3N_4/CdS nanocomposite was optimized. The photocurrent intensity increased with decreasing concentrations of g-C_3N_4/CdS nanocomposite. Dilution of the concentration to one-quarter the initial concentration resulted in the highest photocurrent intensity. Meanwhile, further diluting the concentration of g-C_3N_4/CdS nanocomposite caused the photocurrent intensity to decrease, possibly because of the lower amount of photoactive material. Hence, one-quarter of the initial concentration of prepared g-C_3N_4/CdS nanocomposite was subsequently used.

The incubation time of the target u-PA antigen with anti-u-PA was important in the entire detection process. The effects of different incubation times in the presence of 0.1 ng mL^{-1} of u-PA antigen were determined. As shown in Fig. 3B, the photocurrent intensity rapidly decreased with increasing incubation time and maintained a steady value after 60 min. Therefore, a 60 min u-PA incubation time was selected for subsequent experiments.

3.3. Photoelectrochemical and EIS behavior

To demonstrate the superiority of the prepared g-C_3N_4/CdS nanocomposite, pure g-C_3N_4 and CdS QDs were used as the photoactive materials. As shown in Fig. 4A, curve a, the photocurrent intensity of pure g-C_3N_4 was very low and close to zero. The photocurrent intensity of pure CdS was approximately 20 μA. Curve c in Fig. 4A shows the photocurrent intensity of the g-C_3N_4/CdS nanocomposite. Clearly, the photocurrent intensity of nanocomposite was higher than that of pure g-C_3N_4 and CdS QDs. Thus, we applied the g-C_3N_4/CdS nanocomposite in the following experiments.

The fabrication processes of the photoelectrochemical biosensor can be described by EIS. The semicircular diameter of EIS is the

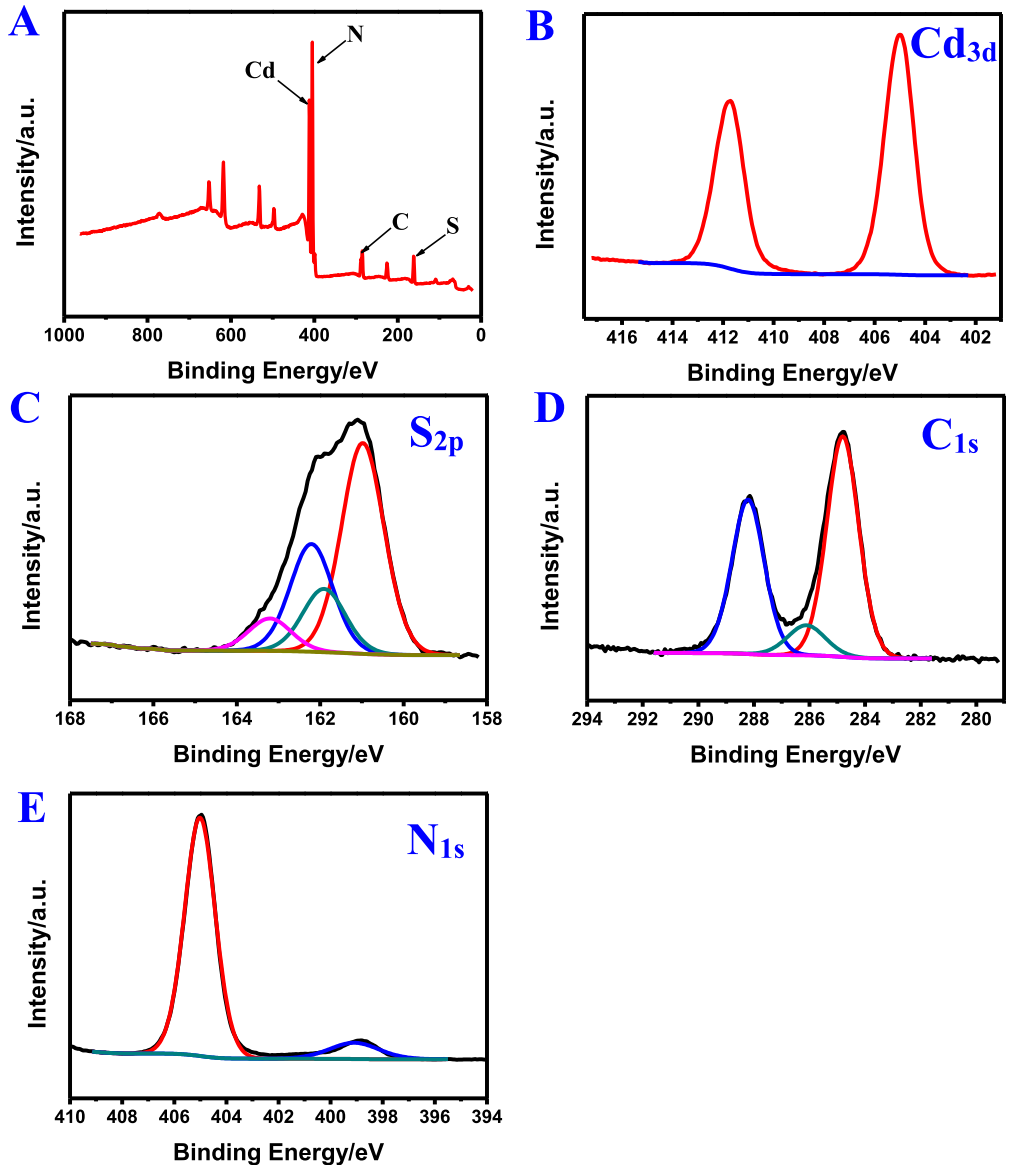

Fig. 2. XPS spectra of the g-C_3N_4/CdS nanocomposite. (A) Survey spectra, (B) Cd_{3d} spectra, (C) S_{2p} spectra, (D) C_{1s} spectra, (E) N_{1s} spectra.

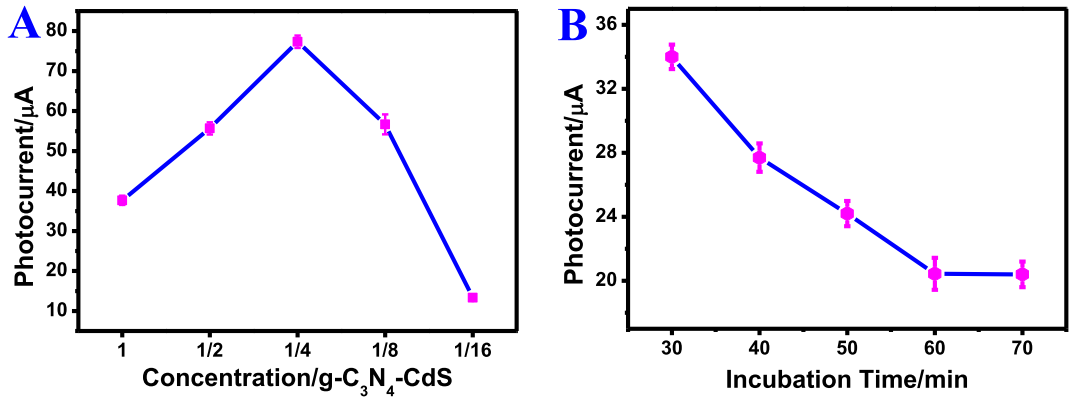

Fig. 3. Effects of (A) the concentration of g-C_3N_4/CdS nanocomposite and (B) the incubation time of u-PA antigens.

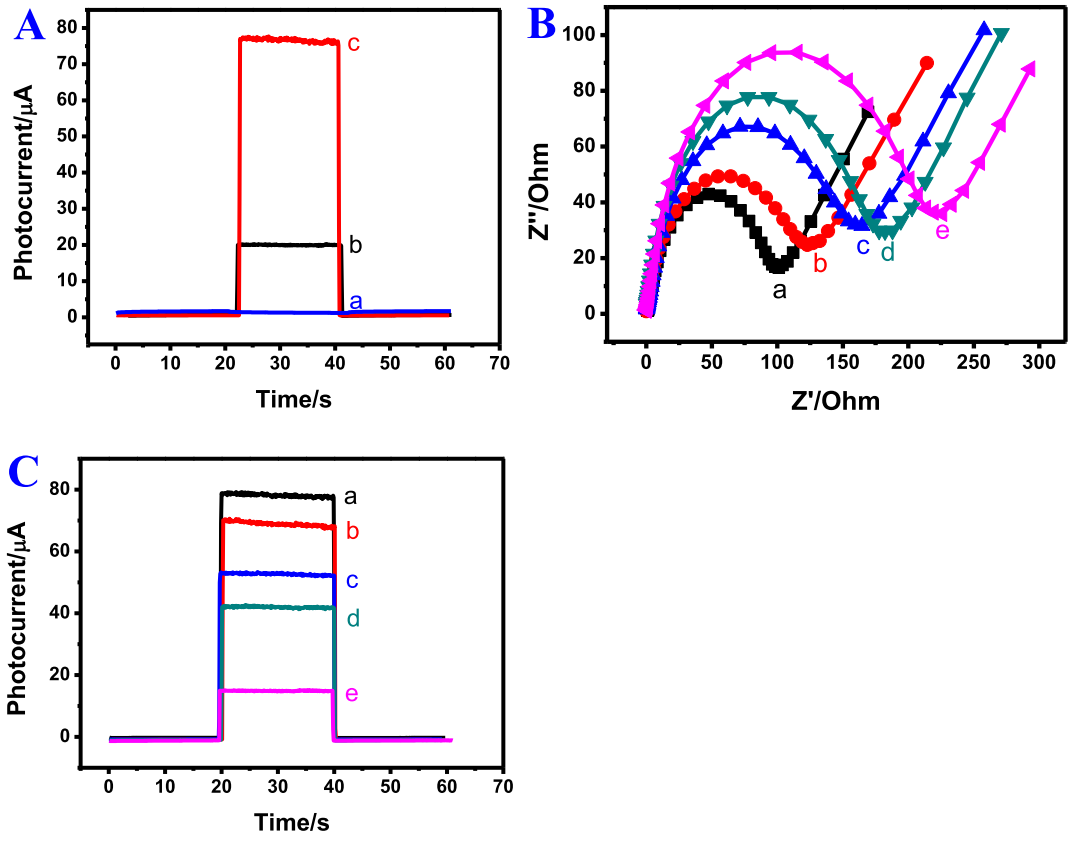

Fig. 4. (A) Photocurrent intensity of different photoactive materials: (a) pure g-C_3N_4, (b) pure CdS and (c) g-C_3N_4/CdS nanocomposite, (B) EIS and (C) corresponding photocurrent intensity for the stepwise biosensor fabrication: (a) FTO/g-C_3N_4/CdS, (b) FTO/g-C_3N_4/CdS/chitosan, (c) FTO/g-C_3N_4/CdS/chitosan/Ab, (d) FTO/g-C_3N_4/CdS/chitosan/Ab/BSA, (e) FTO/g-C_3N_4/CdS/chitosan/Ab/BSA/Ag.

electron-transfer resistance, which represents the electron transfer situation in the assembly process. As shown in Fig. 4B, the FTO/g-C_3N_4/CdS electrode displayed a relatively small electron-transfer resistance (curve a, electron-transfer resistance (R_{et}) = 101 Ω). After the electrode was covered with chitosan, the resistance increased, a result that could be ascribed to the insulating effect of organic molecules (curve b, R_{et} = 123 Ω) [46]. Subsequently, anti-u-PA and the blocking agent BSA were covalently bound to the electrode surface, and the resistance increased gradually, owing to the low conductivity of proteins. These results demonstrated that the assembly of the biosensor was successful (curve c, R_{et} = 164 Ω; curve d, R_{et} = 182 Ω). After the electrode was immobilized with target u-PA antigens, the resistance increased further, thus indicating that the anti-u-PA and u-PA antigens had combined successfully (curve e, R_{et} = 243 Ω). The EIS spectrum confirmed that the fabrication of the photoelectrochemical biosensor was successful.

The photocurrent signal responses of the photoelectrochemical biosensor in different fabrication steps was monitored. As shown in Fig. 4C, the FTO/g-C_3N_4/CdS electrode exhibited a relatively high photocurrent intensity (curve a, I = 77 μA), because the direct band gap of g-C_3N_4 matched the energy levels of CdS QDs, which could effectively suppress the recombination of photo-generated electron-hole pairs and extend their light-capturing ability [17,18]. After the electrode was covered with chitosan, anti-u-PA, and BSA, the photocurrent intensity decreased to 68 μA, 53 μA, and 42 μA (curve b, curve c, and curve d, respectively). This result can be ascribed to the fabrication of those materials sectionally impeded the reaction of AA and photogenerated holes. When the biosensor electrode was incubated with 30 μL of 0.1 μg mL^{-1} target u-PA antigen, the photocurrent response signal decreased significantly (curve e, I = 15.5 μA), which indicated that the target u-PA antigens had combined with anti-u-PA successfully. The photoelectrochemical measurement results were in agreement with the EIS results, thereby further confirming that the fabrication of the biosensor was successful.

3.4. Photoelectrochemical detection of target u-PA

Under the optimal conditions, modified electrodes were applied to assemble the photoelectrochemical biosensor for u-PA detection. The photocurrent intensity of the proposed biosensor was directly related to the concentration of target u-PA. Fig. 5A shows the photocurrent intensity of the biosensor after incubation with different concentrations of target u-PA antigens. After target u-PA incubation, the photocurrent intensity decreased with increasing concentrations of target u-PA antigen. As shown in Fig. 5B, the photocurrent intensity decreased gradually with increasing target u-PA antigen log concentrations in the range of 0.1 pg mL^{-1}–1 μg mL^{-1}. The regression equation was I (μA) = 23.3967–3.9012 log $C_{u\text{-}PA}$/ng·mL^{-1} (n = 3), and the linearly dependent coefficient was 0.9977. The detection limit of the proposed biosensor for u-PA was estimated to be 33 fg mL^{-1}.

3.5. Reproducibility, specificity and stability

Reproducibility is crucial for photoelectrochemical biosensors and plays an important role in analytical methods. The reproducibility of the photoelectrochemical biosensor was assessed by analyzing the detection results of three replicate determinations.

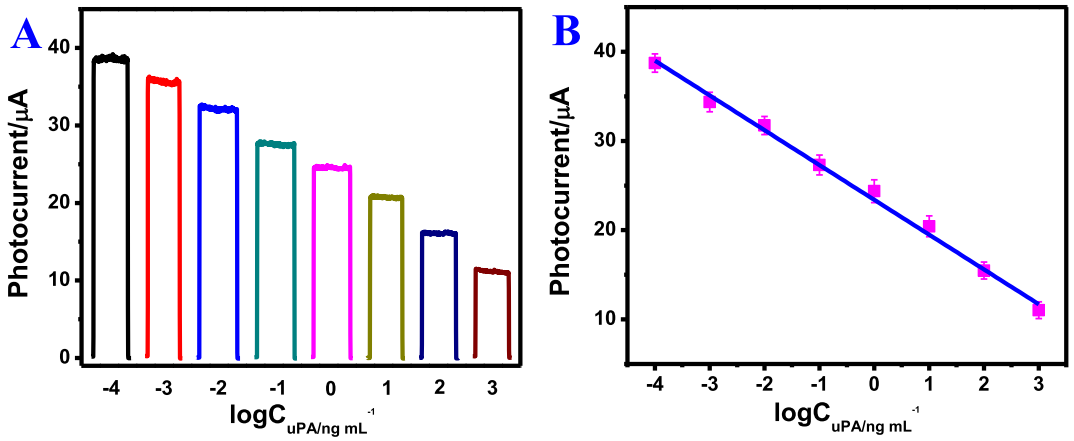

Fig. 5. (A) Photocurrent response and (B) the corresponding calibration curve of the biosensor for the detection of different concentrations of u-PA from 0.1 pg mL^{-1} to 1 μg mL^{-1}.

The relative standard deviation (RSD) was 1.27% towards 10 ng mL^{-1} of u-PA antigen, which indicated that the reproducibility of the designed photoelectrochemical biosensor for detecting target antigen was acceptable.

Specificity is an important index for biosensors and affects the sensitivity of photoelectrochemical biosensors. Thus, the specificity of the designed biosensor was investigated by using the modified electrode for IL-6, CEA, Cyt C, MUC1, and mixture detections. As shown in Fig. 6, the photocurrent intensity of the biosensor for 10 ng mL^{-1} of target u-PA antigen (h) displayed a greater decrease than that of the blank test (a). After replacement of u-PA with IL-6 (b), CEA (c), Cyt C (d), MUC1 (e), or AA (f) the photocurrents of the designed biosensor were much closer to that of the blank test. After the biosensor was incubated with u-PA (10 ng mL^{-1}) containing 100 ng mL^{-1} of various types of the above interfering substances (g), the photocurrent intensity showed almost no change compared with the biosensor incubated with target u-PA only. These results demonstrated that the proposed photoelectrochemical biosensor possessed good selectivity for target u-PA detection.

The storage stability of the photoelectrochemical biosensor for target u-PA detection was also investigated. After the photoelectrochemical biosensor was stored in a refrigerator at 4 °C for more than 2 weeks, the photocurrent response maintained 96% of its initial intensity, thus indicating that the designed photoelectrochemical biosensor possessed good storage stability.

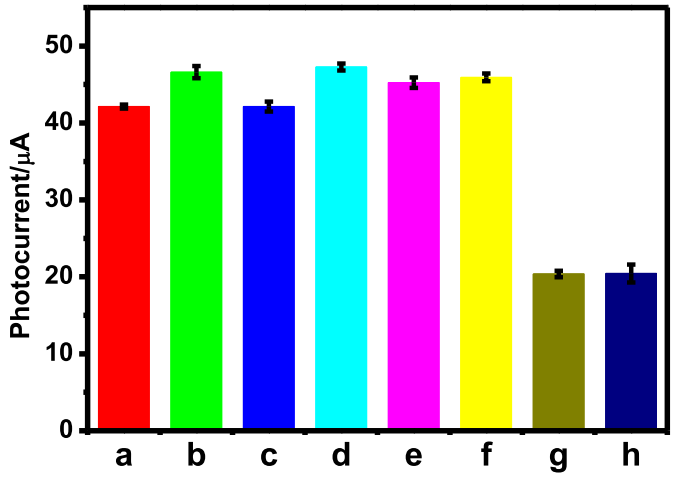

Fig. 6. Selectivity of the proposed photoelectrochemical biosensor with different targets: (a) blank, (b) 100 ng mL^{-1} of IL-6, (c) 100 ng mL^{-1} of CEA, (d) 100 ng mL^{-1} of Cyt C, (e) 100 ng mL^{-1} of MUC1, (f) 100 ng mL^{-1} of AA, (g) a mixture containing 100 ng mL^{-1} of IL-6, CEA, Cyt C, MUC1 and AA of u-PA in the presence of u-PA (10 ng mL^{-1}) and (h) 10 ng mL^{-1} of u-PA.

3.6. Application to detection of real samples

The designed biosensor was used to detect u-PA antigens in human serum through the standard addition method, and the serum samples were diluted ten folds with PBS (10 mM, pH = 7.4) before used. First of all, the matrix effect of human serum was evaluated, after the biosensor electrodes were incubated with pure human serum, the photocurrents were similar to blank test. The result demonstrated that pure serum sample has no significant effect for proposed biosensor. Then tenfold-diluted serum samples with a series of standard concentrations u-PA (0.1, 1, and 10 ng·mL-1) were used. The recovery levels for the added u-PA with different concentrations were 95.33%, 95.67%, and 96.17%, respectively (shown in Table 1), thus indicating that the proposed photoelectrochemical biosensor was an acceptable tool for u-PA detection in complex environments.

4. Conclusions

In summary, a new ultrasensitive photoelectrochemical biosensor for target u-PA antigen detection, based on FTO/g-C_3N_4/CdS electrodes, was assembled successfully. The promising photoelectrochemical biosensor was used for target u-PA detection and found to be highly efficient. This photoelectrochemical biosensor possessed the favorable characteristics of a wide detection range from 0.1 pg mL^{-1} to 1 μg mL^{-1} as well as a low detection limit of 33 fg mL^{-1} for target u-PA detection. Owing to its good specificity, sensitivity, reproducibility, and storage stability, the proposed photoelectrochemical biosensor has promise for the detection of target u-PA, and has further potential for applications in detection and bioanalysis of other antigens.

Table 1
Determination of u-PA added in 10 fold-diluted human serum (n = 3) with the proposed biosensor.

Serum samples	Added (ng·mL^{-1})	Found (ng·mL^{-1})	Recovery (%)	RSD (%)
1	0.1	0.09533	95.33%	1.60%
2	1	0.9567	95.67%	3.96%
3	10	9.617	96.17%	3.69%

Acknowledgments

This work was supported by the National Natural Science Foundation of China (Grant Nos. 21471001, 21427807, 21575001).

References

[1] P.J. Hohensinner, N. Takacs, C. Kaun, B. Thaler, K.A. Krychtiuk, S. Pfaffenberger, A. Aliabadi, A. Zuckermann, K. Huber, J. Wojta, Urokinase plasminogen activator protects cardiac myocytes from oxidative damage and apoptosis via hOGG1 induction, Apoptosis 22 (2017) 1048–1055.
[2] J. Ma, G.W. Qi, J. Xu, H.B. Ni, W.L. Xu, G.Q. Ru, Z.S. Zhao, W.J. Xu, X.J. He, Overexpression of forkhead box M1 and urokinase-type plasminogen activator in gastric cancer is associated with cancer progression and poor prognosis, Oncol. Lett. 14 (2017) 7288–7296.
[3] D. Brungs, J.L. Chen, M. Aghmesheh, K.L. Vine, T.M. Becker, M.G. Carolan, M. Ranson, The urokinase plasminogen activation system in gastroesophageal cancer: a systematic review and meta-analysis, Oncotarget 8 (2017) 23099–23109.
[4] Y.Q. Li, R.X. Yang, Z.H. Li, B. Tian, X.Y. Zhang, J.C. Wang, L.L. Zheng, B.L. Wang, L.H. Li, Urokinase vs Tissue-Type Plasminogen activator for Thrombolytic evacuation of spontaneous intracerebral hemorrhage in Basal ganglia, Front. Neurol. 8 (2017) 371–378.
[5] V. Stepanova, K.V. Dergilev, K.R. Holman, Y.V. Parfyonova, Z.I. Tsokolaeva, M. Teter, E.N. Atochina-Vasserman, A. Volgina, S.V. Zaitsev, S.P. Lewis, F.G. Zabozlaev, K. Obraztsova, V.P. Krymskaya, D.B. Cines, Urokinase-type plasminogen activator (uPA) is critical for progression of tuberous sclerosis complex 2 (TSC2)-deficient tumors, J. Biol. Chem. 292 (2017) 1–33.
[6] L. Wang, Y. Zhang, W.G. Wang, Y.J. Zhu, Y. Chen, B.L. Tian, Gemcitabine treatment induces endoplasmic reticular (ER) stress and subsequently upregulates urokinase plasminogen activator (uPA) to block mitochondrial-dependent apoptosis in Panc-1 cancer stem-like cells (CSCs), PLoS One 12 (2017) 1–18.
[7] K. Zhao, Y. Liu, Z. Xiong, L. Hu, C.L. Xiong, Tissue-specific inhibition of urokinase-type plasminogen activator expression in the testes of mice by inducible lentiviral RNA interference causes male infertility, Reprod. Fertil. Dev. 29 (2017) 2149–2156.
[8] H. Yamamoto, R. Okada, R. Tanaka, K. Unno, K. Lguchi, Expression of a urokinase-type plasminogen activator during tumor growth leads to angiogenesis via galanin activation in tumor-bearing mice, Febs. Open. Bio 7 (2017) 1784–1792.
[9] S. Sinharay, C.M. Howison, A.F. Baker, M.D. Pagel, Detecting in vivo urokinase plasminogen activator activity with a catalyCEST MRI contrast agent, NMR Biomed. 30 (2017) 3721–3728.
[10] A. Diaz, P. Merino, L.G. Marique, J.P. Ospina, L.H. Cheng, F. Wu, V. Jeanneret, M. Yepes, A cross-talk between neuronal urokinase-type plasminogen activator (uPA) and astrocytic uPA receptor (uPAR) promotes astrocytic activation and synaptic recovery in the ischemic brain, J. Neurosci. 37 (2017) 1617–1630.
[11] M.E. Cortina, S. Litwin, M.R. Hawila, S. Miranda, 2017. Multparity upregulates placental plasminogen and urokinasetype plasminogen actvator, Am J Report Immunol 77 (2017) 12633–12643.
[12] M. Roldán-Olarte, V. Maillo, M.J. Sánchez-Calabuig, P. Betrán-Breña, D. Rizos, A. Gutiérrez-Adán, Effect of urokinase type plasminogen activator on in vitro bovine oocyte maturation, Reproduction 54 (2017) 231–240.
[13] M.M. Luan, L.H. Yu, Y.H. Li, W. Pan, X.N. Gao, X.Y. Wan, N. Li, B. Tang, Visualizing breast cancer cell proliferation and invasion for assessing drug efficacy with a fluorescent nanoprobe, Anal. Chem. 89 (2017) 10601–10607.
[14] J. Čejková, Č. Čejka, J. Zvárová, Effects of inhibition of urokinase-type plasminogen activator (U-PA) by amiloride in the cornea and tear fluid of eyes irradiated with UVB, Acta. Histochem. 107 (2005) 77–86.
[15] Y. Wang, Y.L. Zhou, L. Xu, Z.W. Han, H.S. Yin, S.Y. Ai, Photoelectrochemical apta-biosensor for zeatin detection based on graphene quantum dots improved photoactivity of graphite-like carbon nitride and streptavidin induced signal inhibition, Sensor. Actuator. B Chem. 257 (2018) 237–244.
[16] H.Y. Wang, P. Liu, W.J. Jiang, X. Li, H.S. Yin, S.Y. Ai, Photoelectrochemical immunosensing platform for M. SssI methyltransferase activity analysis and inhibitor screening based on g-C_3N_4 and CdS quantum dots, Sensor. Actuator. B Chem. 244 (2017) 458–465.
[17] H.Y. Wang, Q.H. Zhang, H.S. Yin, M.H. Wang, W.J. Jiang, S.Y. Ai, Photoelectrochemical immunosensor for methylated RNA detection based on g-C_3N_4/CdS quantum dots heterojunction and Phos-tag-biotin, Biosens. Bioelectron. 95 (2017) 124–130.
[18] K.Y. Zhang, S.Z. Lv, Z.Z. Lin, D.P. Tang, CdS: Mn quantum dot-functionalized g-C_3N_4 nanohybrids as signalgeneration tags for photoelectrochemical immunoassay of prostate specific antigen coupling DNAzyme concatamer with enzymatic biocatalytic precipitation, Biosens. Bioelectron. 95 (2017) 34–40.
[19] Y. Zhang, N. Hao, Z. Zhou, R. Hua, J. Qian, Q. Liu, H.N. Li, K. Wang, A potentiometric resolved ratiometric photoelectrochemical aptasensor, Chem. Commun 53 (2017) 5810–5813.
[20] B. Zhang, H.Y. Meng, X. Wang, J. Li, H.H. Chang, W.L. Wei, Fe^{3+} doped ZnO-Ag photocatalyst for photoelectrochemical sensing platform of ultrasensitive Hg^{2+} detection using exonuclease III-assisted target recycling and DNAzyme-catalyzed amplification, Sensor. Actuator. B Chem. 255 (2017) 2531–2537.
[21] Z.L. Qiu, J. Shu, D.P. Tang, Near-infrared-to-ultraviolet light-mediated photoelectrochemical aptasensing platform for cancer biomarker based on core-shell NaYF4:Yb,Tm@TiO_2 upconversion microrods, Anal. Chem. 90 (2018) 1021–1028.
[22] B. Wang, Y.X. Dong, Y.L. Wang, J.T. Cao, S.H. Ma, Y.M. Liu, Quenching effect of exciton energy transfer from CdS: Mn to Au nanoparticles: a highly efficient photoelectrochemical strategy for microRNA-21 detection, Sens, Actuator B Chem 254 (2018) 159–165.
[23] H.M. Da, H.Y. Liu, Y.N. Zheng, R. Yuan, Y.Q. Chai, A highly sensitive $VEGF_{165}$ photoelectrochemical biosensor fabricated by assembly of aptamer bridged DNA networks, Biosens. Bioelectron. 101 (2018) 213–218.
[24] Y. Wang, P.P. Wang, Y. Wu, J.W. Di, A cathodic "signal-on" photoelectrochemical sensor for Hg^{2+} detection based on ion-exchange with ZnS quantum dots, Sensor. Actuator. B Chem. 254 (2018) 910–915.
[25] Y. Zang, J.P. Lei, H.X. Ju, Principles and applications of photoelectrochemical sensing strategies based on biofunctionalized nanostructures, Biosens. Bioelectron. 96 (2017) 8–16.
[26] Q. Zhou, Y.X. Lin, M.H. Lu, D.P. Tang, Bismuth ferrite-based photoactive materials for the photoelectrochemical detection of disease biomarkers coupled with multifunctional mesoporous silica nanoparticles, J. Mater. Chem. B 5 (2017) 9600–9607.
[27] C.H. Wang, D.D. Qin, D.L. Shan, J. Gu, Y. Yan, J. Chen, Q.H. Wang, C.H. He, Y. Li, J.J. Quan, X.Q. Lu, Assembly of g-C_3N_4-based type II and Z-scheme heterojunction anodes with improved charge separation for photoelectrojunction water oxidation, Phys. Chem. Chem. Phys. 19 (2017) 4507–4515.
[28] Z. Chen, G. Ma, Z.H. Chen, Y.G. Zhang, Z. Zhang, J.W. Gao, Q.G. Meng, M.Z. Yuan, X. Wang, J.M. Liu, G.F. Zhou, Fabrication and photoelectrochemical properties of silicon nanowires/g-C_3N_4 core/shell arrays, Appl. Surf. Sci. 396 (2017) 609–615.
[29] Y.X. Dong, J.T. Cao, B. Wang, S.H. Ma, Y.M. Liu, Spatial-resolved photoelectrochemical biosensing array based on a CdS@g-C3N4 heterojunction: a universal immunosensing platform for accurate detection, ACS Appl. Mater. Interfaces 10 (2018) 3723–3731.
[30] Z.Z. Tian, S.F. Wang, Y.T. Wang, X.R. Ma, K.T. Cao, D.D. Peng, X.Y. Wu, H. Wu, Z.Y. Jiang, Enhanced gas separation performance of mixed matrix membranes from graphitic carbon nitride nanosheets and polymers of intrinsic microporosity, J. Membr. Sci. 378 (2016) 393–397.
[31] X.H. Pang, H.J. Bian, W.J. Wang, C. Liu, M.S. Khan, Q. Wang, J.N. Qi, Q. Wei, B. Du, A bio-chemical application of N-GQDs and g-C_3N_4 QDs sensitized TiO_2 nanopillars for the quantitative detection of pcDNA3-HBV, Biosens. Bioelectron. 91 (2017) 456–464.
[32] M. Zhao, G.C. Fan, J.J. Chen, J.J. Shi, J.J. Zhu, Facile preparation of exposed {001} facet TiO_2 nanobelts coated by monolayer carbon and its highperformance photocatalytic activity, Anal. Chem. 87 (2015) 12340–12347.
[33] B. Wang, J.T. Cao, Y.X. Dong, F.R. Liu, X.L. Fu, S.W. Ren, S.H. Ma, Y.M. Liu, An in situ electron donor consumption strategy for photoelectrochemical biosensing of proteins based on ternary Bi_2S_3/Ag_2S/TiO_2 NT arrays, Chem. Commun 54 (2018) 806–809.
[34] Q. Liu, Y.J. Peng, J.C. Xu, C. Ma, L.L. Li, C.J. Mao, J.J. Zhu, Label-free electrochemiluminescence aptasensor for highly sensitive detection of acetylcholinesterase based on Au nanoparticles functionalized g-C_3N_4 nanohybrid, ChemElectroChem 4 (2017) 1768–1774.
[35] C. Sun, M.H. Zhang, Q.Q. Fei, D.Y. Wang, Z.L. Sun, Z.M. Geng, W.M. Xu, F. Liu, Graphite-like g-C_3N_4-F127-Au nanosheets used for sensitive monitoring of heat shock protein 90, Sensor. Actuator. B Chem. 256 (2017) 160–166.
[36] J. Xu, Y. Chen, Y. Hong, H. Zheng, D. Ma, B. Xue, Y.X. Li, Direct catalytic hydroxylation of benzene to phenol catalyzed by vanadia supported on exfoliated graphitic carbon nitride, Appl. Catal. A-Gen 549 (2018) 31–39.
[37] T.Y. Ma, Y.H. Tang, S. Dai, S.Z. Qiao, Proton-functionalized two-dimensional graphitic carbon nitride nanosheet: an excellent metal-/label-free biosensing platform, Small 10 (2014) 2382–2389.
[38] E. Nosheen, S.M. Shah, Z. Lqbal, Ru-dye grafted CdS and reduced graphene oxide Ru/CdS/rGO composite: an efficient and photo tuneable electrode material for solid state dye sensitized polymer solar cells, J. Photochem. Photobiol., B 167 (2017) 117–127.
[39] M. Faraz, M. Shakir, N. Khare, Highly sensitive and selective detection of picric acid using a one pot biomolecule inspired polyindole/CdS nanocomposite, New J. Chem. 41 (2017) 5784–5793.
[40] K.S. Prasad, T. Amin, S. Katuva, M. Kumari, K. Selvaraj, Synthesis of water soluble CdS nanoparticles and study of their DNA damage activity, Arab. J. Chem. 10 (2014) 3929–3935.
[41] S.W. Cao, Y.P. Yuan, J. Fang, M.M. Shahjamali, F.Y.C. Boey, J. Barber, S.C.J. Loo, C. Xue, In-situ growth of CdS quantum dots on g-C_3N_4 nanosheets for highly efficient photocatalytic hydrogen generation under visible light irradiation, Int. J. Hydrogen Energy 38 (2013) 1258–1266.
[42] T.F. Wu, P.F. Wang, J. Qian, Y.H. Ao, C. Wang, J. Hou, Noble-metal-free nickel phosphide modified CdS/C_3N_4 nanorods for dramatically enhanced photocatalytic hydrogen evolution under visible light irradiation, Dalton Trans. 46 (2017) 13793–13801.
[43] Y.X. Dong, J.T. Cao, B. Wang, S.H. Ma, Y.M. Liu, Exciton–plasmon interactions

between CdS@g-C3N4 heterojunction and Au@Ag nanoparticles coupled with DNAase-triggered signal amplification: toward highly sensitive photoelectrochemical bioanalysis of microRNA, ACS Sustain. Chem. Eng. 5 (2017) 10840–10848.

[44] Y.V. Fedoseeva, V.E. Arkhipov, E.A. Maksimovskiy, A.V. Gusel'nikov, Y.L. Mikhlin, K.S. Zhuravlev, B.V. Senkovskiy, S.V. Larionov, L.G. Bulusheva, A.V. Okotrub, Fluorinated surface of carbon nanotube buckypaper for uniform growth of CdS nanoparticles, J. Phys. Chem. C 121 (2017) 19182–19190.

[45] D.D. Chen, J.Z. Fang, S.Y. Lu, G.Y. Zhou, W.H. Feng, F. Yang, Y. Chen, Z.Q. Fang, Fabrication of Bi modified Bi2S3 pillared g-C_3N_4 photocatalyst and its efficient photocatalytic reduction and oxidation performances, Appl. Surf. Sci. 426 (2017) 427–436.

[46] G.C. Fan, X.L. Ren, C. Zhu, J.R. Zhang, J.J. Zhu, A new signal amplification strategy of photoelectrochemical immunoassay for highly sensitive interleukin-6 detection based on TiO_2/CdS/CdSe dual co-sensitized structure, Biosens. Bioelectron. 59 (2014) 45–53.